Gel–Liposome-Mediated Co-Delivery of Anticancer Membrane-Associated Proteins and Small-Molecule Drugs for Enhanced Therapeutic Efficacy

Tianyue Jiang, Ran Mo, Adriano Bellotti, Jianping Zhou, and Zhen Gu**

A programmed drug-delivery system that can transport different anticancer therapeutics to their distinct targets holds vast promise for cancer treatment. Herein, a core–shell-based "nanodepot" consisting of a liposomal core and a crosslinked-gel shell (designated Gelipo) is developed for the sequential and site-specific delivery (SSSD) of tumor necrosis factor-related apoptosis-inducing ligand (TRAIL) and doxorubicin (Dox). As a small-molecule drug intercalating the nuclear DNA, Dox is loaded in the aqueous core of the liposome, while TRAIL, acting on the death receptor (DR) on the plasma membrane, is encapsulated in the outer shell made of crosslinked hyaluronic acid (HA). The degradation of the HA shell by HAase that is concentrated in the tumor environment results in the rapid extracellular release of TRAIL and subsequent internalization of the liposomes. The parallel activity of TRAIL and Dox show synergistic anticancer efficacy. The half-maximal inhibitory concentration (IC_{50}) of TRAIL and Dox co-loaded Gelipo (TRAIL/Dox-Gelipo) toward human breast cancer (MDA-MB-231) cells is 83 ng mL^{-1} (Dox concentration), which presents a 5.9-fold increase in the cytotoxicity compared to 569 ng mL^{-1} of Dox-loaded Gelipo (Dox-Gelipo). Moreover, with the programmed choreography, Gelipo significantly improves the inhibition of the tumor growth in the MDA-MB-231 xenograft tumor animal model.

1. Introduction

Combination therapy holds considerable appeal in enhancement of antitumor activity by achieving synergistic effects and reducing toxicity, which has been proved to be more effective than monotherapy in preclinical and clinical cancer treatment.[1–3] However, the general administration of agent "cocktails" based combination therapy often suffers from distinct pharmacokinetic profiles of different therapeutics that lead to an inconsistent in vivo biodistribution and therefore an inefficient therapy.[4,5] To address this dilemma, the nanoparticle-based drug co-delivery systems, such as polymeric nanoparticles,[6–8] liposomes,[9] nanocomplex[10–12] and inorganic nanoparticles,[13–15] have been widely developed to unify the individual pharmacokinetic behavior of different drug cargos. Upon the enhanced permeability and retention (EPR) effect, a single nanocarrier preferentially transports the multiple therapeutic agents, either small-molecule drugs or macromolecular drugs with different antitumor mechanisms to the same destination.

The conventional chemotherapeutic drugs attack the tumors by interrupting processes or inhibiting substances essential for the replication and proliferation of the tumor cells. For example, co-delivery of doxorubicin (Dox) and paclitaxel (Ptx) by a polymeric nanoparticle[16] was able to release both drugs simultaneously and efficiently within the cells. The released Ptx inhibits the intracytoplasmic microtubules disassembly that is required for cell proliferation,[17] while Dox intercalates into the nuclear DNA and induced cell apoptosis.[18] For the cancer gene therapy, siRNA for silencing the target genes in cancer cells and pDNA for implanting corrective genetic material into the cells, have been applied to coordinate with small-molecule drugs.[7,12] A typical example involves a micellar nanocarrier for co-delivery of MDR-1 siRNA and Dox, the released siRNA in the cells downregulates the P-glycoprotein expression to improve the efficacy of Dox in the multidrug-resistant cancer cells.[7]

Protein therapeutics such as cytokines,[19–21] antibodies,[22,23] and transcription factors[24] are emerging anticancer strategies, typically based on two mechanisms: apoptosis signal activation[21] and growth signal blockage.[25] Of note, these proteins have specific sites of activities, which are generally divided as the extracellular target on the cellular membrane and the intracellular object in the cells. For example, cytochrome c[26] and caspase 3[27] act in the cytosol to initiate activation of

T. Jiang, Dr. R. Mo, A. Bellotti, Prof. Z. Gu
Joint Department of Biomedical Engineering,
University of North Carolina at Chapel Hill and
North Carolina State University
Raleigh, NC, 27695, USA
Tel: (+1) 919–515–7944
E-mail: zgu@email.unc.edu or zgu3@ncsu.edu
T. Jiang, Dr. R. Mo, Prof. Z. Gu
Molecular Pharmaceutics Division
Eshelman School of Pharmacy
University of North Carolina at Chapel Hill
Chapel Hill, NC, 27599, USA
T. Jiang, Dr. R. Mo, Prof. J. Zhou
State Key Laboratory of Natural Medicines
China Pharmaceutical University
Nanjing, 210009, China
E-mail: zhoujianp@cpu.edu.cn

DOI: 10.1002/adfm.201303222

the caspase cascade for the intrinsic apoptosis pathway;[28] while some take effect by binding to the specific receptor on the plasma membrane, such as cetuximab to the human epidermal growth factor receptor (EGFR),[29,30] trastuzumab to the human epidermal growth factor receptor 2 (HER-2),[31] and tumor necrosis factor (TNF)-related apoptosis-inducing ligand (TRAIL) to the death receptor.[20,21] However, a synergistic anticancer co-delivery system integrating membrane-associated proteins and intracellular-functioned small-molecule drugs still remains elusive.

Herein, we report a novel core-shell based nano-vehicle for sequential and site-specific delivery (SSSD) of an anticancer protein and a small-molecule drug, which act on the cellular membrane and in the nucleus, respectively. As shown in **Figure 1**A, to achieve a programmed release profile, a core-shell complex is designed to incorporate two separate depots: 1) a liposome based inner core for loading the small-molecule drug and 2) a crosslinked gel based outer shell for encapsulating the therapeutic protein. The materials used to compose these depots are tailored to arm with the stimuli-responsive elements that can be degraded or dissociated upon distinct tumor microenvironmental and cellular conditions. We therefore hypothesize that the obtained gel-liposome complex (designated "Gelipo") undergoes sequential triggers to precisely release cargoes into different specific sites. To demonstrate our hypothesis, two kinds of anticancer agents, Dox and TRAIL were applied. As a model small-molecule drug that functions by intercalating the nuclear DNA,[18] Dox is encapsulated in the aqueous core of the cell-penetrating peptide (CPP, R8H3) modified liposome (R8H3-L). TRAIL induces apoptosis primarily in the tumor cells by binding to certain death receptors (DR4, DR5) on the plasma membrane, while exhibits insignificant toxicity to the normal cells.[32] Enzymatically degradable hyaluronic acid (HA) modified with acrylated pendants was utilized to adhere to the R8H3-L surface and subsequently encapsulate oppositely charged TRAIL into a photo-crosslinked matrix, which enhances protein stability, avoids denaturation in plasma, and shields from immunogenicity.[33] Furthermore, the HA shell also provides the active tumor targeting ligand to bind the overexpressing receptors on the cell surface of a variety of tumors, such as CD44 receptor.[34,35]

As displayed in Figure 1B, after intravenous injection (i.v.) of TRAIL and Dox co-loaded Gelipo (TRAIL/Dox-Gelipo), Gelipo is expected to exhibit a considerable accumulation at the tumor site due to a combination of passive and active targeting mechanisms. At the tumor microenvironment, hyaluronidase (HAase), a specific enzyme has been proved to be highly expressed,[36,37] which promotes the degradation of the HA shell, thereby allowing the release of TRAIL and the exposure of R8H3-L. The extracellular released TRAIL binds to the cell death receptor on the plasma membrane, which can activate the cellular signaling to induce programmed cell death.[38,39] On

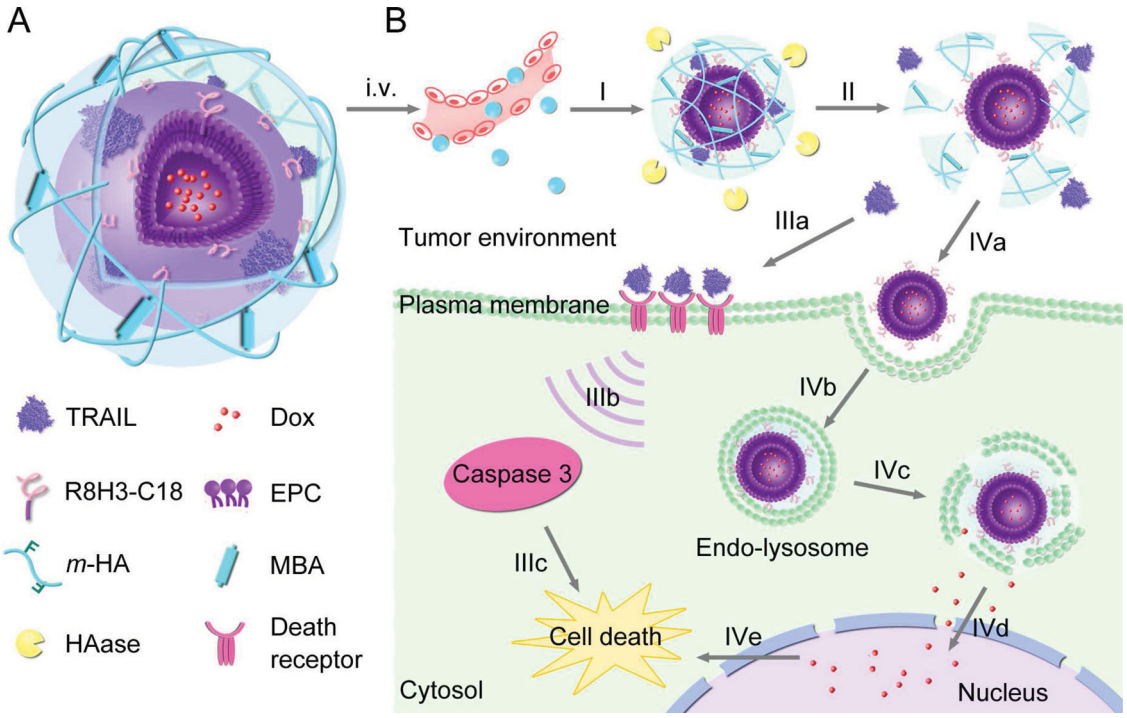

Figure 1. Schematic design of TRAIL/Dox-Gelipo for sequential and site-specific drug delivery. A) The main components of TRAIL/Dox-Gelipo: R8H3 modified liposomal core loading Dox and crosslinked HA gel based outer shell encapsulating TRAIL. B) Sequential delivery of TRAIL to the plasma membrane and Dox to the nuclei by TRAIL/Dox-Gelipo for combination cancer treatment. I, accumulation of Gelipo (blue balls) at the tumor site through the passive and active targeting effects; II, degradation of HA crosslinked shell by HAase; IIIa, released TRAIL binding onto the death receptors on the plasma membrane; IIIb, activation of the caspase 3 signaling pathway; IIIc, induction of the cell death; IVa, exposure of R8H3 facilitating the tumor cellular uptake of Dox-R8H3-L; IVb, internalization of Dox-R8H3-L into the tumor cells; IVc, endo-lysosomal escape; IVd, accumulation of the released Dox into nucleus; IVe, intercalation of Dox on DNA inducing the cell death.

the other hand, the exposed positively charged R8H3 improves the internalization efficiency of the liposome into the tumor cells. When localized into endosomes and lysosomes (endo-lysosomes), Dox-R8H3-L is able to efficiently transport from the endo-lysosomes with the help of R8H3 possessing high cell-penetrating capability, accompanied by the release of Dox. The released Dox specifically accumulates into the nuclei for subsequent trigger of the apoptosis and cytotoxicity.[18,40]

2. Results and Discussion

2.1. Preparation and Characterization of Gelipo

We first prepared Dox-loaded liposomes (Dox-L) as the liposomal core of Gelipo by the transmembrane pH gradient method.[41] The drug-loading capacity and the encapsulation efficiency of Dox in Dox-L were about 5% and 99.5%, respectively, showing that Dox was efficiently encapsulated in the hydrophilic inner core of the liposomes. Dox-L had an average diameter of about 76 nm and a zeta potential of –14 mV (**Figure 2**A). Next, the positively charged TRAIL with a molecular weight of about 24 KDa (Figure S1, Supporting information) was attached onto the surface of negatively charged Dox-L via electrostatic absorption (TRAIL/Dox-L) (Figure S2, Supporting Information), which resulted in a slight decrease of the zeta potential to –10 mV. A synthesized CPP (R8H3) conjugated with a stearyl chain (R8H3-C18) was then anchored into the membrane of TRAIL/Dox-L by a combination of hydrophobic and electrostatic interactions[42] (TRAIL/Dox-R8H3-L) determined by a significant charge conversion from -10 mV of TRAIL/Dox-L to +26 mV of TRAIL/Dox-R8H3-L. Finally, TRAIL/DOX-Gelipo was obtained by adding TRAIL/Dox-R8H3-L into a solution with the negatively charged HA modified with polymerizable acrylate groups (designated *m*-HA) (Figure S3, Supporting Information) and a crosslinker, *N,N'*-methylenebisacrylamide (MBA) followed by the interfacial polymerization[43] via UV irradiation for a short period of time. The notably increased particle diameter of 120 nm and a highly negative surface charge of –22 mV indicated the successful coating of the HA-crosslinked gel shell on the surface of the liposomal core. The encapsulation efficiency of TRAIL in TRAIL/Dox-R8H3-L was determined to be 82%. The transmission electron microscope (TEM) image showed a spheroid structure of TRAIL/Dox-Gelipo with a uniform particle size of about 110 nm (Figure 2B).

To verify the degradation of the HA crosslinked shell by HAase rich in the tumor microenvironment, the changes in the particle size and zeta potential of TRAIL/Dox-Gelipo were monitored after incubation with HAase at pH 6.5 (the typical tumor extracellular pH) over time. As shown in Figure 2C, the particle size of TRAIL/Dox-Gelipo reduced sharply from 125 nm to 105 nm in the first 5 min, and continuously decreased to 83 nm within 1 h, which was attributed to the degraded small molecular HA fragments shedding from Gelipo. Moreover, After a 1 h incubation with HAase, the surface charge of the Gelipo reversed from –20 mV to +10 mV, suggesting that the

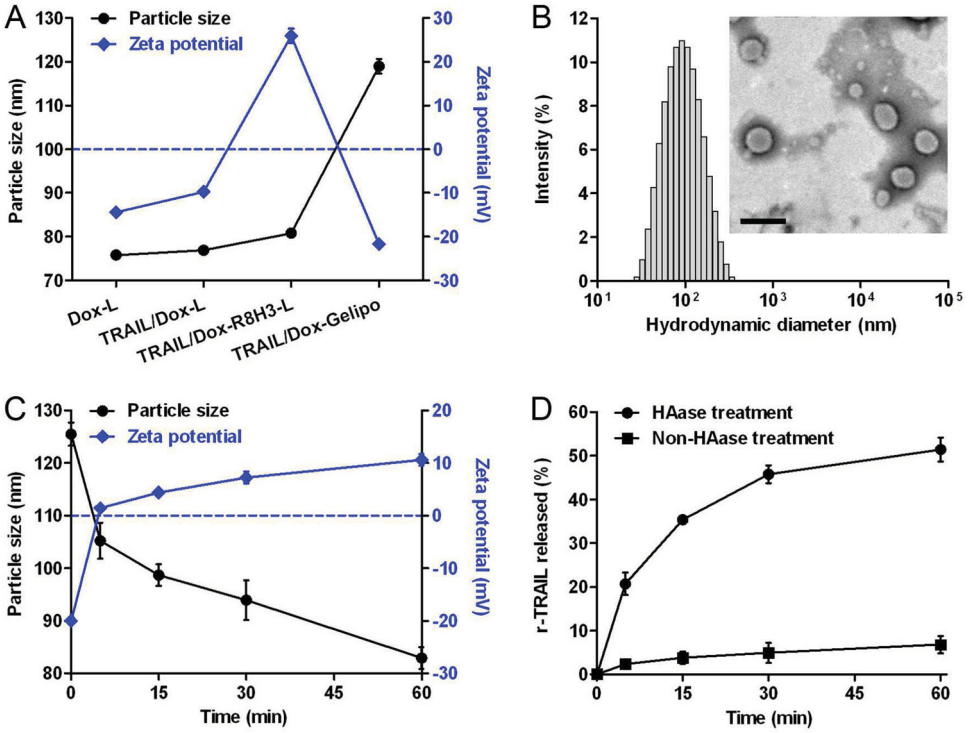

Figure 2. A) The particle size and zeta potential of Dox-L, TRAIL/Dox-L, TRAIL/Dox-R8H3-L and TRAIL/Dox-Gelipo. B) The hydrodynamic size of TRAIL/Dox-Gelipo measured by dynamic light scattering (DLS). Inset: TEM image of TRAIL/Dox-Gelipo. Scale bar is 200 nm. C) Change in particle size and zeta potential of Gelipo incubated with HAase at pH 6.5 over time. D) In vitro release of r-TRAIL from r-TRAIL-Gelipo with and without HAase treatment.

HA shell degradation of Gelipo led to the exposure of positively charged R8H3-L, the liposomal core of Gelipo, which plays a significant role in the enhancement on the tumor cellular uptake.[44,45] More importantly, the degradation of the HA shell by HAase facilitates the release of TRAIL from TRAIL/Dox-Gelipo at the tumor site, which can subsequently bind to the DR on the cellular surface to induce apoptosis. To evaluate the HAase-mediated release of TRAIL, we investigated the in vitro release profile of rhodamine-labeled TRAIL (r-TRAIL) from Gelipo without Dox (r-TRAIL-Gelipo) in the presence and absence of HAase at pH 6.5 at 37 °C. As shown in Figure 2D, only 2.3% of r-TRAIL was released from r-TRAIL-Gelipo in the first 5 min and about 6.8% was released within 1 h in the absence of HAase. In contrast, the presence of HAase accelerated the release of r-TRAIL from r-TRAIL-Gelipo. After incubation with HAase, 20.7% of r-TRAIL was released from r-TRAIL-Gelipo in the first 5 min and more than 50% was released within 1 h. Furthermore, the circular dichroism (CD) spectrum of the released TRAIL was in agreement with that of the native TRAIL (Figure S4, Supporting information), indicating that there were no noticeable conformational changes in the secondary structure of TRAIL during the process of the assembly and disassembly of Gelipo. Accordingly, it was demonstrated that HAase, rich in the tumor extracellular matrix, can degrade the HA shell of Gelipo, which was determined by the size reduction and charge conversion, thereby promoting the release of TRAIL toward the cellular membrane for initiation of death signaling and simultaneously allowing the exposure of R8H3 for enhanced cellular uptake.

2.2. Site-Specific Delivery of TRAIL and Dox by Gelipo

To validate that the released TRAIL from the degraded HA shell of the Gelipo can efficiently bind onto the tumor cellular membrane, the human breast adenocarcinoma (MDA-MB-231) cells were incubated with r-TRAIL-Gelipo with or without HAase pre-treatment at different temperatures for 1 h followed by observation using the confocal laser scanning microscope (CLSM). The endocytosis of the nanoparticle is inhibited at 4 °C,[46] while both the internalization and membrane binding occurred at 37 °C. As shown in **Figure 3**A, there was a remarkable difference in the distribution of r-TRAIL from r-TRAIL-Gelipo without HAase treatment between at 4 °C and at 37 °C. A significantly larger amount of red rhodamine fluorescence was localized onto the green fluorescent cellular membrane than within the cells at 4 °C, which implied that the endocytosis of Gelipo was inhibited by lowering the temperature and Gelipo was only able to bind on the plasma membrane. However, at 37 °C, most of red rhodamine fluorescence was detected within the cells, indicating that the encapsulated r-TRAIL in Gelipo can be easily transported into the cells via the endocytosis of Gelipo by the cells. In sharp contrast, after 30 min HAase treatment, a great majority of red fluorescence of r-TRAIL was apparently dispersed on the cellular membrane. Furthermore, the quantitative assay substantiated that 80% of r-TRAIL was determined to have bound onto the membrane after HAase treatment, 4-fold that within the cells, whereas without HAase treatment, a higher amount of r-TRAIL in the cells was detected than that on the membrane (Figure 3B). It was therefore confirmed that the degradation of the HA shell of Gelipo by HAase leads to a rapid release of TRAIL at the tumor site, which can efficiently bind onto the tumor cellular membrane to trigger the following extrinsic apoptosis pathway.

Next, the intracellular delivery of TRAIL/Dox-Gelipo after HAase treatment in MDA-MB-231 cells was further investigated using CLSM. Gelipo was demonstrated to be internalized by the cells via a combination of clathrin-dependent endocytosis and macropinocytosis-mediated engulfment (Figure S5, Supporting Information) following binding to the CD44 receptor (Figure S6, Supporting Information), and subsequently be localized into the endosomes and lysosomes.[47–49] As shown in Figure 3C, a large number of the endocytosed Gelipo was located in the green fluorescent endo-lysosomes, evidenced by the overlaid yellow fluorescence during the first 1 h of incubation. Nevertheless, after 4 h of incubation, an evident separation of the red fluorescent Gelipo and the green fluorescent endo-lysosomes was observed, which indicated that Gelipo efficiently escaped from the endo-lysosomes with the assistance of R8H3 possessing a high cell penetrating capability (Figure S7, Supporting Information). Of note, the released Dox from Gelipo (Figure S8, Supporting Information) specifically accumulated into the blue fluorescent nuclei judged by the merged magenta fluorescence, which plays an important role in activation of the intrinsic apoptosis pathway. Collectively, Gelipo is able to sequentially release TRAIL and Dox upon the characteristics of the tumor extracellular and intracellular conditions, which can efficiently deliver the released TRAIL and Dox to their distinct sites for anticancer activities.

2.3. In vitro Synergistic Apoptosis and Cytotoxicity

Based on the site-specific delivery of TRAIL and Dox by Gelipo, the apoptosis-inducing activity of the released TRAIL through the degradation of HA shell of Gelipo was first explored toward MDA-MB-231 cells using the Annexin-FITC apoptosis detection assay. As shown in **Figure 4**A, after 12 h of cell incubation, free TRAIL (20 ng/mL) showed a strong capability of inducing apoptosis, which had an apoptosis ratio of 51.71% and a viability of 32.30%. TRAIL-Gelipo without Dox after HAase treatment had an apoptosis-inducing capability comparable to free TRAIL. In contrast, the viability increased to 58.01% and the apoptosis ratio decreased to 39.58% when the cells were incubated with TRAIL-Gelipo without pre-treatment of HAase. It was suggested that HAase-mediated TRAIL release from Gelipo contributed to the distribution of TRAIL onto the membrane similar to that of free TRAIL for maximizing apoptosis activity, whereas without HAase treatment, the endocytosis of Gelipo with the encapsulated TRAIL into the cells relatively reduced the apoptosis-inducing ability of TRAIL.

We then evaluated the synergistic apoptosis-inducing effect of TRAIL and Dox by Gelipo on MDA-MB-231 cells. As shown in Figure 4A, either free TRAIL (2 ng/mL) or Dox-R8H3-L (100 ng/mL) showed the apoptosis-inducing characteristics, and the apoptosis ratios were 36.48% and 38.52%, respectively. Of note, HAase-treated TRAIL/Dox-Gelipo at a fixed concentration ratio of 2 ng/mL TRAIL and 100 ng/mL Dox had a prominent

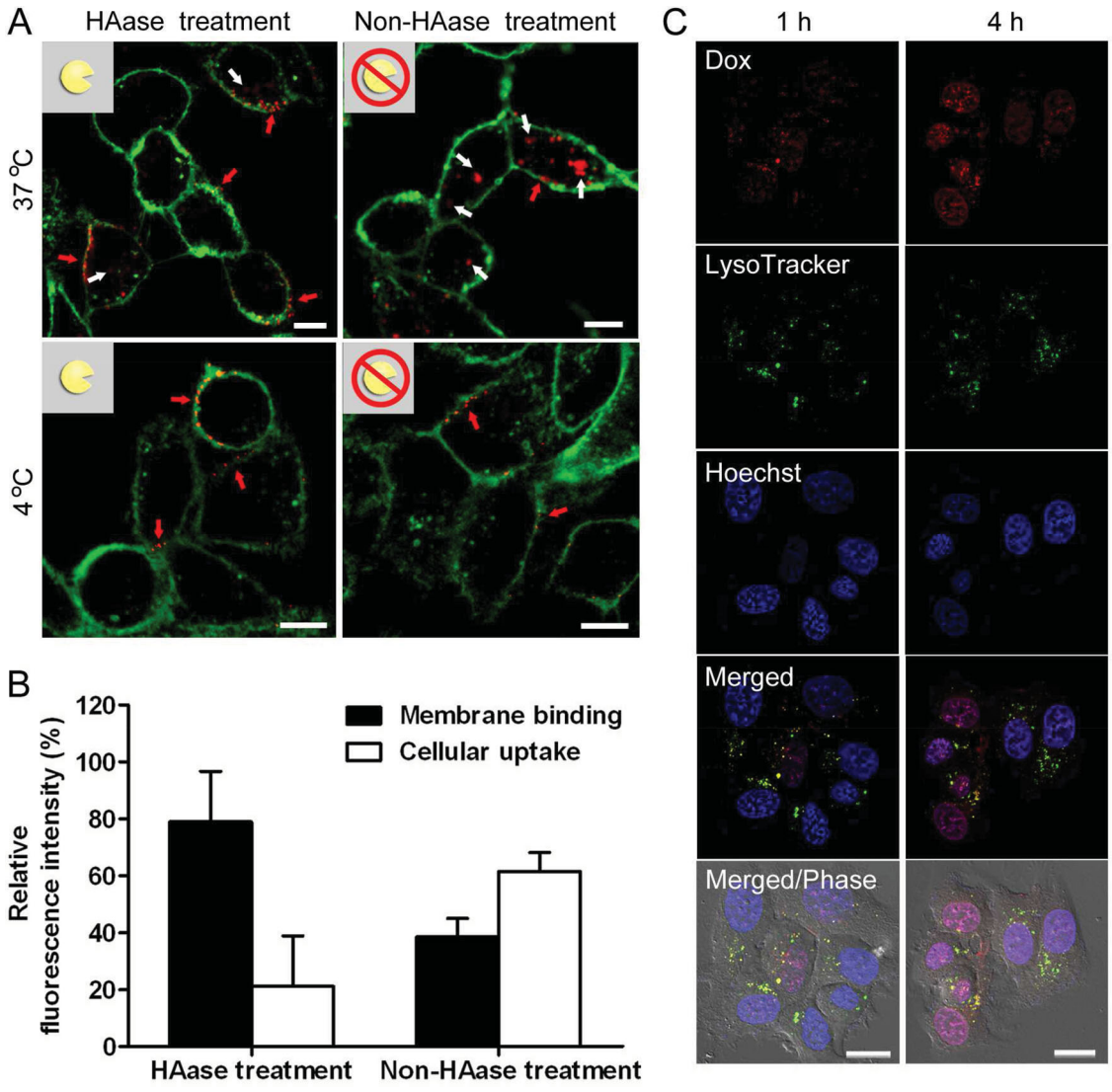

Figure 3. A) Membrane binding efficiency of r-TRAIL from r-TRAIL-Gelipo with and without 30 min of HAase pre-treatment on MDA-MB-231 cells observed by CLSM. The plasma membranes were stained by Alexa Fluor 488 conjugate of wheat germ agglutinin (WGA). Scale bars are 10 μm. B) Quantitative analysis on the r-TRAIL amount on the plasma membrane and in the cells. C) Intracellular delivery of TRAIL/Dox-Gelipo after 30 min of HAase pre-treatment on MDA-MB-231 cells at different time observed by CLSM. The late endosomes and lysosomes were stained by LysoTracker Green, and the nuclei were stained by Hoechst 33342. Scale bars are 20 μm.

apoptosis ratio higher than 80%. In addition, assessed by the terminal deoxynucleotidyl transferase dUTP nick end labeling (TUNEL) assay, MDA-MB-231 cells incubated with HAase-treated TRAIL/Dox-Gelipo exhibited broader apoptotic DNA fragmentation stained as green fluorescence compared to that treated with the single therapeutics, free TRAIL or Dox-R8H3-L alone (Figure 4B). These results substantiated that TRAIL/Dox-Gelipo has a synergistic induction of apoptosis toward the cancer cells through the combination efficacy of TRAIL and Dox.

The in vitro cytotoxicity of TRAL/Dox-Gelipo against MDA-MB-231 cells was evaluated by using the 3-(4,5-dimethylthiazol-2-yl)-2,5-diphenyltetrazolium bromide (MTT) assay. As shown in Figure 4C, the half-maximal inhibitory concentration (IC_{50}) of HAase-treated Dox-loaded Gelipo (Dox-Gelipo) without TRAIL was 569 ng/mL on MDA-MB-231 cells, which showed 1.2-fold increase in the cytotoxicity compared to 1279 ng/mL of Dox-L without R8H3 decoration (Figure S9, Supporting Information), indicating that R8H3 promotes the efficient intracellular delivery of the liposomes. More importantly, TRAIL/Dox-Gelipo after HAase treatment displayed a significantly greater cytotoxicity against MB-MDA-231 cells with the IC_{50} of 83 ng/mL (Dox concentration). Additionally, the bare R8H3-L and Gelipo without TRAIL and Dox showed negligible toxicities within all the tested concentrations (Figure 4D). Consequently, the combination delivery of TRAIL and Dox to their primary activity sites provides a high potential for improved cytotoxicity.

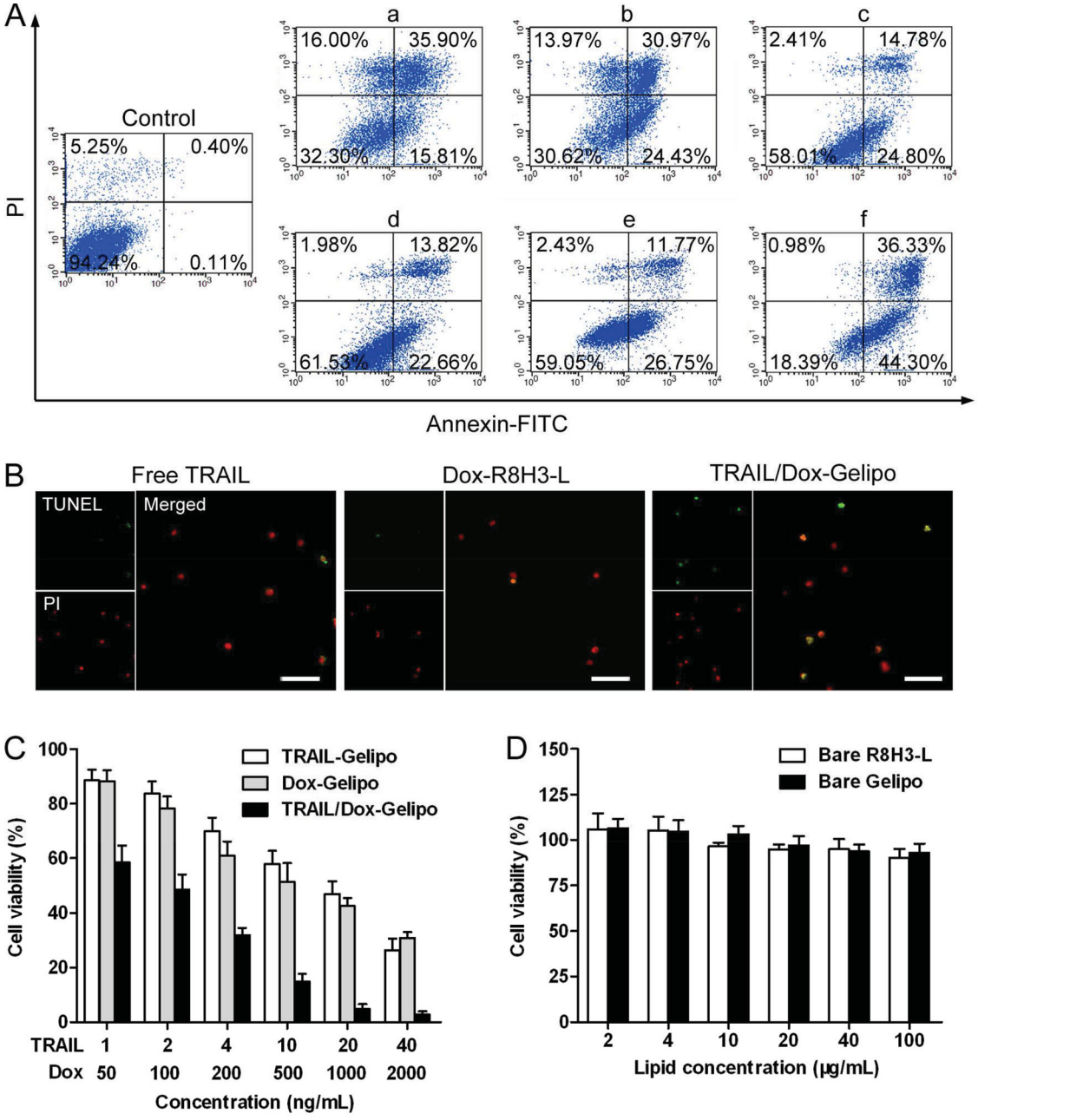

Figure 4. A) Flow cytometric analysis of MDA-MB-231 cell apoptosis induced by different formulations for 12 h by using Annexin V-FITC/PI staining. a, free TRAIL (20 ng/mL); b, TRAIL-Gelipo (20 ng/mL) after 30 min of HAase pre-treatment; c, TRAIL-Gelipo (20 ng/mL) without HAase pre-treatment; d, free TRAIL (2 ng/mL); e, Dox-R8H3-L (100 ng/mL); TRAIL/Dox-Gelipo (2 ng/mL TRAIL, 100 ng/mL Dox) after 30 min of HAase pre-treatment. B) MDA-MB-231 cell apoptosis induced by free TRAIL (2 ng/mL), Dox-R8H3-L (100 ng/mL) and TRAIL/Dox-Gelipo (2 ng/mL TRAIL, 100 ng/mL Dox) after a 30 min of HAase pre-treatment for 18 h using the APO-BrdU TUNEL assay. Alexa Fluor 488-stained nick end label showed green fluorescence, and PI-stained nuclei showed red fluorescence. Scale bar is 100 μm. C) In vitro cytotoxicity of TRAIL-Gelipo, Dox-Gelipo and TRAIL/Dox-Gelipo after 30 min of HAase pre-treatment toward MDA-MB-231 cells for 24 h. D) In vitro cytotoxicity of the bare R8H3-L and Gelipo toward MDA-MB-231 cells for 24 h.

2.4. In vivo Targetability and Antitumor Efficacy

To estimate the targetability of Gelipo in vivo, the biodistribution of Cy5.5-labeled TRAIL (Cy5.5-TRAIL) loaded Gelipo (Cy5.5-TRAIL-Gelipo) administrated intravenously into the MB-MDA-231 tumor-implanted nude mice was monitored by a non-invasive near infrared optical imagining technique. As shown in **Figure 5**A, Cy5.5-TRAIL-Gelipo exhibited a stronger Cy5.5 signal at the tumor site at 4 h post-injection. As time extended, a higher fluorescence signal was clearly observed in the tumor region compared with that in the normal tissues at 48 h post-injection, validating the significant tumor targeting

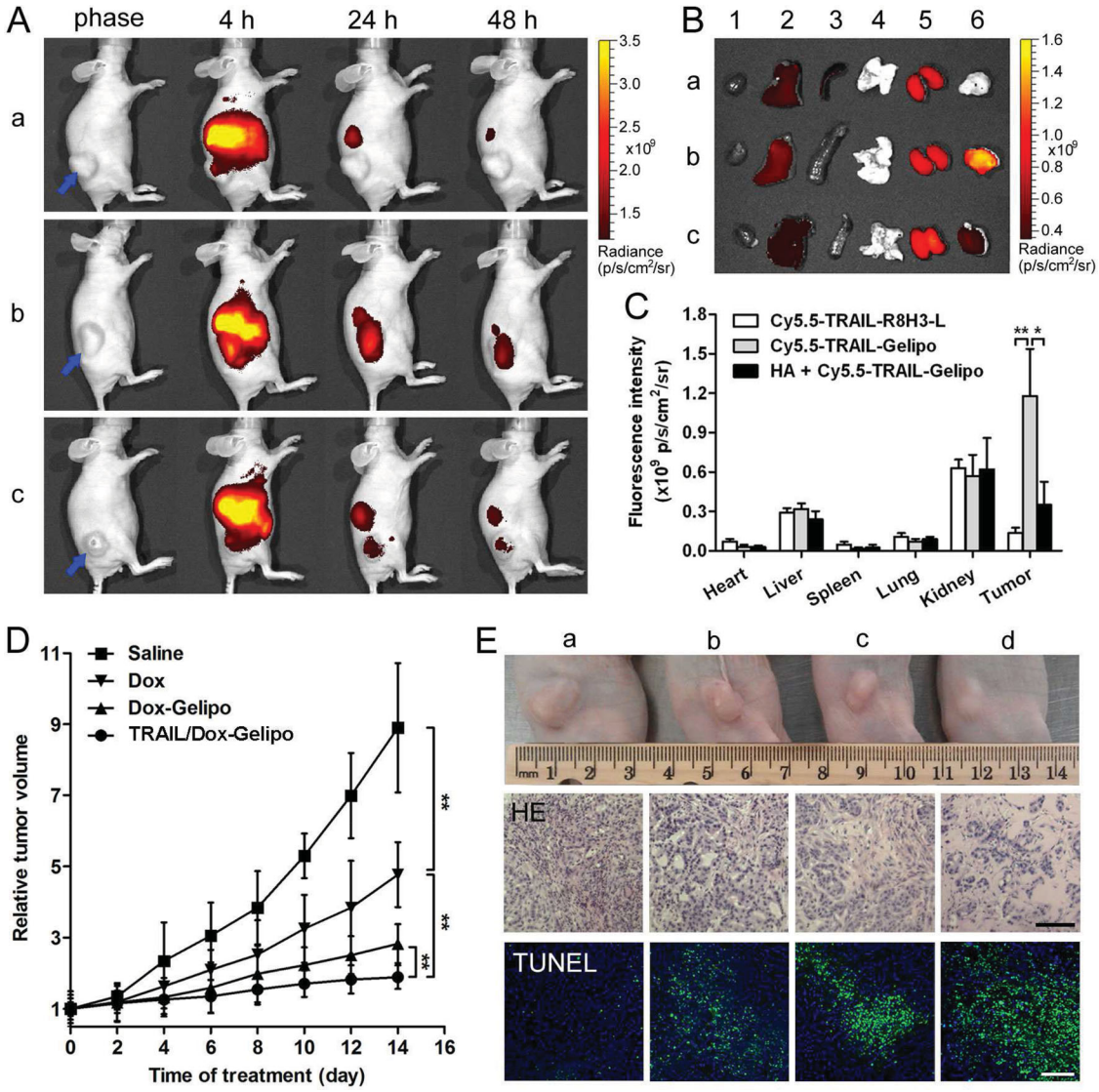

Figure 5. A) In vivo fluorescence imaging of the MDA-MB-231 tumor-bearing nude mice at 4, 24, and 48 h after intravenous injection of Cy5.5-TRAIL-R8H3-L (a), Cy5.5-TRAIL-Gelipo (b) and Cy5.5-TRAIL-Gelipo with pre-injection of free HA (c) at Cy5.5 dose of 30 nmol/kg. The arrows indicate the regions of the tumors. B) Ex vivo fluorescence imaging of the tumor and normal tissues of the MDA-MB-231 tumor-bearing nude mice after mice were euthanized at 48 h post-injection. 1, heart; 2, liver; 3, spleen; 4, lung; 5, kidney; 6, tumor. C) ROI analysis of fluorescent signals from the tumors and normal tissues. $^{*}P < 0.05$, $^{**}P < 0.01$. D) The MDA-MB-231 tumor growth curves after intravenous injection of different formulations of Dox at a dose of 2 mg/kg. $^{**}P < 0.01$. E) Representative images of MDA-MB-231 xenograft tumors of the mice after treatment with saline (a), the Dox solution (b), Dox-Gelipo (c) and TRAIL/Dox-Gelipo (d) at Day 14; Histological observation of the tumor tissues after treatment. The tumor sections were stained with HE. Scale bar is 100 μm; Detection of apoptosis in the tumor tissues after treatment. The tumor sections were stained with fluorescein-dUTP (green) for apoptosis and Hoechst for nuclei (blue). Scale bar is 100 μm.

effect of Gelipo. However, almost no signal at the tumor site was imaged after a 48 h injection of Cy5.5-TRAIL-R8H3-L without HA coating, which mainly resulted from a rapid clearance of cationic liposomes.[50] To further confirm the role of the HA shell in the active targeting of Gelipo to CD44 overexpressing tumor, a high dose of HA polymer was injected before the administration of Gelipo. As expected, a conspicuous attenuation of Cy5.5 signal at the tumor site was visualized at all the time points, revealing that the HA shell not only retained the stability of Gelipo in the systemic circulation but also endued Gelipo with the active tumor targetability. After 48 h imaging, the tumor and normal tissues were separated from the mice after euthanasia for ex vivo imaging. As shown in Figure 5B, the strongest Cy5.5 signal was observed at the tumor tissue after applying Cy5.5-TRAIL-Gelipo compared to Cy5.5-TRAIL-R8H3-L and Cy5.5-TRAIL-Gelipo pretreated with HA, and this fluorescence signal was much higher than that at the normal tissues. The quantitative region-of-interest (ROI) analysis determined that Cy5.5-TRAIL-Gelipo had the fluorescence intensity at the tumor site 8.6-fold and 3.4-fold that of

Cy5.5-TRAIL-R8H3-L and Cy5.5-TRAIL-Gelipo pretreated with HA, respectively, as well as 2.7-fold and 1.1-fold increase compared to that in the liver and kidney, respectively (Figure 5C).

We also evaluate the in vivo biodistribution of the Dox solution, Dox-R8H3-L and TRAIL/Dox-Gelipo after intravenous administration into the MB-MDA-231 tumor-bearing mice by quantitatively detecting the Dox amounts in plasma and different tissues, including heart, liver, spleen, lung, kidney and tumor. TRAIL/Dox-Gelipo showed an enhanced blood persistence compared with the Dox solution (Figure S10, Supporting Information), which suggested that Gelipo was able to support a high concentration of Dox within a longer time in the systemic circulation for improved therapeutic index. Moreover, TRAIL/Dox-Gelipo provided higher Dox accumulation in the tumor tissues than the Dox solution and Dox-R8H3-L (Figure S11, Supporting Information). The Dox amount in the tumor tissues delivered by TRAIL/Dox-Gelipo was 5.72- and 2.70-fold that of those delivered by the Dox solution and Dox-R8H3-L at 48 h post-injection. Additionally, the Dox amount was 1.66-, 4.55- and 1.24-fold that of those in the liver, spleen and kidney delivered by TRAIL/Dox-Gelipo at 48 h post-injection. Accordingly, it was confirmed that Gelipo had a high tumor targetability as a result of a combination of the passive and active targeting mechanisms.

To demonstrate the feasibility of Gelipo for cancer treatment in vivo, the antitumor activity of Dox/NG was evaluated using MDA-MB-231 tumor xenograft models. As shown in Figure 5D, the tumor growth was remarkably suppressed after the successive intravenous injection of various Dox formulations including the Dox solution, Dox-Gelipo and TRAIL/Dox-Gelipo, compared with saline as a negative control. Dox-Gelipo generated a noticeably higher effect on inhibiting tumor growth than the Dox solution, which mainly resulted from the EPR effect of nanoscaled Gelipo combined with the active targeting capability provided by the HA shell. It is worth noting that TRAIL/Dox-Gelipo showed a dominant effect on tumor inhibition compared with Dox-Gelipo (Figure 5D, E), further validating the synergistic antitumor effect by a combination of TRAIL and Dox. The body weight of mice receiving TRAIL/Dox-Gelipo remained stable during the treatment (Figure S12, Supporting Information). The histologic images of the tumor section stained by the hematoxylin and eosin (HE) showed a massive cancer cell remission after applying TRAIL/Dox-Gelipo (Figure 5E), which offered a considerable evidence of the efficient in vivo antitumor activity of TRAIL/Dox-Gelipo. Moreover, the fluorescence images obtained using the in situ TUNEL assay presented the highest level of cell apoptosis in the tumor collected from the mice receiving TRAIL/Dox-Gelipo (Figure 5E), indicating that the prominent capability of tumor growth inhibition was partly due to the elevated apoptosis activated by TRAIL/Dox-Gelipo. Taken together, it was verified that TRAIL/Dox-Gelipo preferentially accumulated at the tumor site, efficiently delivered the TRAIL and Dox to their specific sites of activity, and thereby accomplished optimal synergistic antitumor efficacy.

3. Conclusions

We successfully developed "Gelipo" with a liposomal core and a crosslinked HA shell for sequential and site-specific delivery (SSSD) of TRAIL and Dox. Gelipo is able to efficiently deliver its cargoes, TRAIL and Dox at the tumor sites in a programmed fashion. At the HAase-rich tumor microenvironment, the HA outer corona of Gelipo was degraded by HAase and peeled off, followed by the extracellular release of TRAIL to bind onto the membrane receptor to trigger the extrinsic apoptosis pathway. Meanwhile, the degradation of the HA shell allowed the exposure of R8H3 with a high cell-penetrating ability, which contributed to the enhanced cellular uptake and efficient intracellular delivery of Dox for activation of the intrinsic apoptosis pathway. Gelipo achieved a synergistic antitumor activity by a combined efficacy of TRAIL and Dox. In addition to TRAIL, other proteins that act on the tumor cellular membrane, such as cetuximab[29] and trastuzumab,[31] could also be loaded in the interspace between the HA shell and the liposomal core and be release by HAase invasion, which provides more opportunities for combination cancer treatment with gene therapy (siRNA, pDNA) or chemotherapy (Dox, Ptx, cisplatin). Our "SSSD" based design strategy will open an avenue for the exploration of more sophisticated DDSs, which can synergistically differentiate the extracellular and intracellular target to promote a superior anticancer effect.

4. Experimental Section

Materials: All chemicals unless mentioned were purchased from Sigma-Aldrich. Stearyl R8H3 (R8H3-C18) as well as FITC-labeled R8H3 (R8H3-FITC) and R8 (R8-FITC) were purchased from the GL Biochem Co., Ltd. (Shanghai, China). Sodium hyaluronic acid (HA, the molecular weight of 77 kDa) was purchased from Freda Biochem Co., Ltd. (Shandong, China). Doxorubicin hydrochloride was purchased from BIOTANG Inc. (Lexington, MA, USA).

Preparation and Characterization of Gel–Liposome (Gelipo): Dox-loaded liposomes (Dox-L) were prepared by the transmembrane pH gradient method. Egg phosphatidylcholine (EPC) and cholesterol (Chol) (5:1, w:w) were dissolved in chloroform, followed by rotation vacuum evaporation at 40 °C to form a thin lipid film. After overnight vaccum dry to remove trace organic solvent, the lipid film was hydrated in 200 mM ammonium sulfate ($(NH_4)_2SO_4$), dispersed by a probe-type ultrasonicator and extruded through the filter membranes with the pore size of 0.45 μm and 0.20 μm successively, followed by dialysis overnight. Then, the blank liposomes were mixed with the Dox solution (Dox:lipids, 1:20, w:w) and incubated at 45 °C for 40 min. The resulting Dox-L was obtained by washing with deionized (DI) water using centrifugal filters (10K MWCO) (Millipore) to remove free Dox. Subsequently, the pre-cold Dox-L was incubated with TRAIL (Dox:TRAIL, 50:1, w:w) at 4 °C for 0.5 h, followed by addition of R8H3-C18 (2.5 mol% of the total lipid weight) and incubation for additional 0.5 h. This solution was then added into the *m*-HA solution (HA:lipids, 3:20, w:w), followed by adding a crosslinker, *N*,*N*-methylenebisacrylamide (MBA) (MBA:*m*-HA, 1:1, w:w) and a photo-initiator Irgacure 2959 (0.1%, w:v). After radical polymerization via UV radiation for 60 s using a BlueWave 75 UV Curing Spot Lamp (DYMAX), TRAIL/Dox-Gelipo was obtained by washing with HEPES buffer (10 mM, pH 7.4) using centrifugal filters (30K MWCO) (Millipore) to remove the excessive crosslinker and initiator. The particle size and zeta potential of TRAIL/Dox-Gelipo were measured by a Zetasizer (Nano ZS, Malvern). For TEM observation, TRAIL/Dox-Gelipo was dropped onto a TEM copper grid (300 mesh) (Ted Pella) and then stained by phosphotungstic acid (1%, v:v). After air-drying, the sample was observed by TEM (JEM-2000FX, Hitachi) operating at 80 kV.

Degradation of HA Shell: 500 μL of Gelipo was incubated with 500 μL of HAase (1 mg/mL) at pH 6.5 in a 37 °C water bath. At predetermined

time intervals, the particle size and zeta potential of the samples were immediately measured by a Zetasizer (Nano ZS, Malvern).

In vitro HAase-Mediated TRAIL Release: 500 μL of rhodamine-labeled TRAIL-loaded Gelipo (r-TRAIL-Gelipo) was incubated with 500 μL of HAase (1 mg/mL) at pH 6.5 in a 37 °C water bath. At prearranged time intervals, free r-TRAIL in the filtrate was harvested using centrifugal filters (30K MWCO) (Millipore). The fluorescence intensity of r-TRAIL was determined at 585 nm with an excitation wavelength of 552 nm by a microplate reader (Infinite M200 PRO, Tecan). Additionally, the far-UV CD spectra of the native TRAIL and the released TRAIL from TRAIL Gelipo were obtained using a Circular Dichroism Spectrometer (Aviv).

Cell Culture: MDA-MB-231 cells were cultured in DMEM containing FBS (10%, v:v), penicillin (100 U/mL) and streptomycin (100 μg/mL) in an incubator (Thermo Scientific) at 37 °C under an atmosphere of 5% CO_2 and 90% relative humidity. The cells were sub-cultivated approximately every 3 days at 80% confluence using trypsin (0.25%, w:v) at a split ratio of 1:5.

Site-Specific Delivery: MDA-MB-231 cells (1×10^5 cells/well) were seeded in a confocal microscopy dish (MatTek) and cultured for 24 h. For the membrane binding assay, the cells were incubated with r-TRAIL-Gelipo (0.2 μg/mL) treated with HAase (1 mg/mL) for 30 min, at 37 °C or 4 °C for 1 h. Afterwards, the cells were washed with ice-cold PBS twice, and stained by Alexa Fluor 488 conjugate of WGA Green (5 μg/mL) (Life Technologies) at 37 °C for 10 min. The cells were washed with ice-cold PBS twice, and immediately observed using CLSM (LSM710, Zeiss).

For quantitative analysis, the cells were incubated with r-TRAIL-Gelipo (0.2 μg/mL) with or without HAase-treament at 37 °C or 4 °C for 1 h. The cells were harvested and washed by ice-cold PBS thrice. The fluorescence intensity of r-TRAIL was measured at 585 nm with an excitation wavelength of 552 nm, which was normalized by subtracting the background signal of the blank cells. The cell proteins were assayed by the Pierce BCA protein assay kit (Thermo Scientific). The amount of r-TRAIL binding on the plasma membrane or internalized within the cells ($U_{\text{r-TRAIL}}$) was calculated as: $U_{\text{r-TRAIL}}$ (ng/mg) = $Q_{\text{r-TRAIL}}/Q_{\text{protein}}$, where $Q_{\text{r-TRAIL}}$ and Q_{protein} were the amounts of r-TRAIL and cellular protein, respectively. $U_{\text{r-TRAIL}}$ after incubation at 37 °C indicated the total amount of r-TRAIL binding on the plasma membrane plus internalized within the cells, while that after incubation at 4 °C referred to the amount of TRAIL binding on the plasma membrane due to the endocytosis inhibition at 4 °C.

For the intracellular delivery study, the cells were incubated with Dox-Gelipo (1 μg/mL) after HAase-treatment at 37 °C for 1 h and 4 h. Then, the cells were washed with ice-cold PBS twice, and stained by LyosTracker Green (50 nM) (Life Technologies) at 37 °C for 30 min and Hoechst 33342 (1 μg/mL) (Life Technologies) at 37 °C for 10 min. The cells were washed by ice-cold PBS twice and immediately observed using CLSM (LSM710, Zeiss).

Cell Apoptosis Assay: Apoptosis of MDA-MB-231 cells was detected using the Annexin V-FITC Apoptosis Detection Kit (BD Biosciences) and APO-BrdU TUNEL Assay Kit (Life Technologies), respectively. The cells (1×10^5 cells/well) were seeded in 6-well plates and cultured for 48 h. For Annexin V-FITC assay, the cells were incubated with different formulations for 12 h, including free TRAIL (2 or 20 ng/mL), TRAIL-Gelipo (20 ng/mL) with or without HAase-treatment, Dox-R8H3-L (100 ng/mL), TRAIL/Dox-Gelipo (2 ng/mL TRAIL, 100 ng/mL Dox) with HAase-treament. For TUNEL assay, the cells were incubated with free TRAIL (2 ng/mL), Dox-R8H3-L (100 ng/mL) and TRAIL/Dox-Gelipo (2 ng/mL TRAIL, 100 ng/mL Dox) with HAase-treament for 20 h, respectively. The following procedures were performed in accordance with the manufacturers' protocols. Finally, for Annexin V-FITC assay, the cells were analyzed by flow cytometry (BD FACSCalibur), while for TUNEL assay, the cells were observed by fluorescence microscope (IX71, Olympus).

In vitro Cytotoxicity: MDA-MB-231 (1×10^4 cells/well) were seeded in 96-well plates and cultured for 24 h. The cells were exposed to TRAIL-Gelipo, Dox-Gelipo and TRAIL/Dox-Gelipo (TRAIL:Dox, 1:50, w:w) after the HAase treatment at different concentrations of Dox for 24 h. 20 μL of the MTT solution (5 mg/mL) was added into each well and the cells was stained for 4 h. Then the medium was removed, and the cells were dissolved in 150 μL of dimethyl sulfoxide (DMSO). The absorbance was measured at a test wavelength of 570 nm and a reference wavelength of 630 nm by a microplate reader (Infinite M200 PRO, Tecan).

Animals and Tumor Xenograft Models: All animals were treated in accordance with the Guide for Care and Use of Laboratory Animals, approved by local committee. The female nude mice were subcutaneously inoculated in the back with MDA-MB-231 cells (1×10^7 cells/mouse) for the construction of the tumor xenograft model. The tumor size was monitored by a fine caliper and the tumor volume (V) was calculated as $V = L \times W^2/2$, where L and W were the length and width of the tumor, respectively.

In vivo Imaging Study: When the tumors reached to 200–400 mm^3, the mice were intravenously injected by Cy5.5-TRAIL-R8H3-L and Cy5.5-TRAIL-Gelipo at Cy5.5 dose of 30 nmol/kg, respectively. For HA competitive study, the mice were injected by Cy5.5-TRAIL-Gelipo at 30 min after pre-injected by a high dose of free HA (50 mg/kg). Images were taken on IVIS Lumina imaging system (Caliper, USA) at 4, 24, and 48 h post injection. After the 48 h imaging, the tumors as well as major organs were collected from the mice after euthanasia and subjected for ex vivo imaging. ROIs were circled around the organs, and the fluorescence intensities were analyzed by Living Image Software.

In vivo Antitumor Efficacy: When the tumor volume reached to 50 mm^3, the mice were weighed, randomly divided into 4 groups, and intravenously administrated with the Dox solution (2 mg/kg), Dox-Gelipo (2 mg/kg), Dox/TRAIL-Gelipo (2 mg/kg Dox, 0.04 mg/kg TRAIL) and saline every other day for 12 days. The tumor size and body weight of the mice were measured at the meantime. At Day 14, the tumor were harvested from the mice after euthanasia, washed by saline thrice and then fixed in 10% neutral buffered formalin (NBF). For HE staining, formalin-fixed tumors were embedded in paraffin blocks and visualized by optical microscope (DM5500B, Leica). For TUNEL apoptosis staining, the fixed tumor sections were stained by the *In Situ* Cell Death Detection Kit (Roche Applied Science) according to the manufacturer's protocol. Hoechst 33342 was used for nuclear nuclear counterstaining. The stained tumor slides were observed by fluorescence microscope (IX71, Olympus).

Statistical Analysis: Data are given as mean ± standard deviation. Statistical significance was tested by two-tailed Student's *t*-test or one-way ANOVA. Statistical significance was set at $^{*}P < 0.05$, and extreme significance was set at $^{**}P < 0.01$.

Supporting Information

Supporting Information is available from the Wiley Online Library or from the author.

Acknowledgements

T. Jiang and R. Mo contributed equally to this work. This work was supported by the start-up package through the Joint Biomedical Engineering Department at NCSU and UNC-CH and the NC State Faculty Research and Professional Development Award to Dr. Gu. We greatly thank Dr. Seulki Lee and Dr. Tae Hyung Kim at Johns Hopkins School of Medicine for offering us *Escherichia coli* containing the pET23dw-His-ILZ-hTRAIL vector as a gift. We also greatly thank Dr. Jonathan Horowitz, Dr. Elizabeth Loboa, Dr. Michael Gamcsik and Dr. Glenn Walker for providing experimental facilities. We acknowledge the use of the Analytical Instrumentation Facility (AIF) at NCSU, which is supported by the State of North Carolina and the National Science Foundation (NSF). We greatly thank the China Scholarship Council for financially supporting T. Jiang's foreign research and life.

Received: September 17, 2013
Revised: November 13, 2013
Published online: January 2, 2014

[1] J. Bergh, I. M. Bondarenko, M. R. Lichinitser, A. Liljegren, R. Greil, N. L. Voytko, A. N. Makhson, J. Cortes, A. Lortholary, J. Bischoff, A. Chan, S. Delaloge, X. Huang, K. A. Kern, C. Giorgetti, *J. Clin. Oncol.* **2012**, *30*, 921.
[2] B. J. Giantonio, P. J. Catalano, N. J. Meropol, P. J. O'Dwyer, E. P. Mitchell, S. R. Alberts, M. A. Schwartz, A. B. Benson, *J. Clin. Oncol.* **2007**, *25*, 1539.
[3] W. J. Gradishar, L. A. Meza, B. Amin, D. Samid, T. Hill, Y.-M. Chen, E. E. Lower, P. K. Marcom, *J. Clin. Oncol.* **2004**, *22*, 2321.
[4] J. Lehar, A. S. Krueger, W. Avery, A. M. Heilbut, L. M. Johansen, E. R. Price, R. J. Rickles, G. F. Short, J. E. Staunton, X. W. Jin, M. S. Lee, G. R. Zimmermann, A. A. Borisy, *Nat. Biotechnol.* **2009**, *27*, 659.
[5] C. M. Hu, S. Aryal, L. Zhang, *Ther. Deliv.* **2010**, *1*, 323.
[6] N. Kolishetti, S. Dhar, P. M. Valencia, L. Q. Lin, R. Karnik, S. J. Lippard, R. Langer, O. C. Farokhzad, *Proc. Natl. Acad. Sci. USA* **2010**, *107*, 17939.
[7] X. B. Xiong, A. Lavasanifar, *ACS Nano* **2011**, *5*, 5202.
[8] S. Aryal, C. M. J. Hu, L. F. Zhang, *Small* **2010**, *6*, 1442.
[9] R. J. Lee, *Mol. Cancer Ther.* **2006**, *5*, 1639.
[10] Y. Liu, J. Du, M. Yan, M. Y. Lau, J. Hu, H. Han, O. O. Yang, S. Liang, W. Wei, H. Wang, J. Li, X. Zhu, L. Shi, W. Chen, C. Ji, Y. Lu, *Nat. Nanotechnol.* **2013**, *8*, 187.
[11] Z. Chen, M. F. Penet, S. Nimmagadda, C. Li, S. R. Banerjee, P. T. Winnard, D. Artemov, K. Glunde, M. G. Pomper, Z. M. Bhujwalla, *ACS Nano* **2012**, *6*, 7752.
[12] S. X. Huang, K. Shao, Y. Liu, Y. Y. Kuang, J. F. Li, S. An, Y. B. Guo, H. J. Ma, C. Jiang, *ACS Nano* **2013**, *7*, 2860.
[13] H. Meng, W. X. Mai, H. Y. Zhang, M. Xue, T. Xia, S. J. Lin, X. Wang, Y. Zhao, Z. X. Ji, J. I. Zink, A. E. Nel, *ACS Nano* **2013**, *7*, 994.
[14] Y. Chen, Y. Gao, H. Chen, D. Zeng, Y. Li, Y. Zheng, F. Li, X. Ji, X. Wang, F. Chen, Q. He, L. Zhang, J. Shi, *Adv. Funct. Mater.* **2012**, *22*, 1586.
[15] C. Wang, H. Xu, C. Liang, Y. Liu, Z. Li, G. Yang, L. Cheng, Y. Li, Z. Liu, *ACS Nano* **2013**, *7*, 6782.
[16] H. Wang, Y. Zhao, Y. Wu, Y. L. Hu, K. H. Nan, G. J. Nie, H. Chen, *Biomaterials* **2011**, *32*, 8281.
[17] H. Lataste, V. Senilh, M. Wright, D. Guenard, P. Potier, *Proc. Natl. Acad. Sci. USA* **1984**, *81*, 4090.
[18] A. Bodley, L. F. Liu, M. Israel, R. Seshadri, Y. Koseki, F. C. Giuliani, S. Kirschenbaum, R. Silber, M. Potmesil, *Cancer Res.* **1989**, *49*, 5969.
[19] G. Dranoff, *Nat. Rev. Cancer* **2004**, *4*, 11.
[20] R. W. Johnstone, A. J. Frew, M. J. Smyth, *Nat. Rev. Cancer* **2008**, *8*, 782.
[21] S. Mocellin, C. R. Rossi, P. Pilati, D. Nitti, *Cytokine Growth Factor Rev.* **2005**, *16*, 35.
[22] G. P. Adams, L. M. Weiner, *Nat. Biotechnol.* **2005**, *23*, 1147.
[23] A. M. Scott, J. D. Wolchok, L. J. Old, *Nat. Rev. Cancer* **2012**, *12*, 278.
[24] A. Phelan, G. Elliott, P. O'Hare, *Nat. Biotechnol.* **1998**, *16*, 440.
[25] A. M. Scott, J. P. Allison, J. D. Wolchok, *Cancer Immun.* **2012**, *12*, 14.
[26] R. M. Kluck, E. BossyWetzel, D. R. Green, D. D. Newmeyer, *Science* **1997**, *275*, 1132.
[27] S. A. Lakhani, A. Masud, K. Kuida, G. A. Porter, , Jr., C. J. Booth, W. Z. Mehal, I. Inayat, R. A. Flavell, *Science* **2006**, *311*, 847.
[28] S. W. Lowe, E. Cepero, G. Evan, *Nature* **2004**, *432*, 307.
[29] S. Q. Li, K. R. Schmitz, P. D. Jeffrey, J. J. W. Wiltzius, P. Kussie, K. M. Ferguson, *Cancer Cell* **2005**, *7*, 301.
[30] N. E. Hynes, H. A. Lane, *Nat. Rev. Cancer* **2005**, *5*, 341.
[31] R. Nahta, M. C. Hung, F. J. Esteva, *Cancer Res.* **2004**, *64*, 2343.
[32] M. M. Keane, S. A. Ettenberg, M. M. Nau, E. K. Russell, S. Lipkowitz, *Cancer Res.* **1999**, *59*, 734.
[33] Z. Gu, A. Biswas, M. X. Zhao, Y. Tang, *Chem. Soc. Rev.* **2011**, *40*, 3638.
[34] B. P. Toole, *Nat. Rev. Cancer* **2004**, *4*, 528.
[35] E. Kim, J. Yang, J. Park, S. Kim, N. H. Kim, J. I. Yook, J. S. Suh, S. Haam, Y. M. Huh, *ACS Nano* **2012**, *6*, 8525.
[36] R. Stern, M. J. Jedrzejas, *Chem. Rev.* **2006**, *106*, 818.
[37] P. Bertrand, N. Girard, C. Duval, J. d'Anjou, C. Chauzy, J. F. Menard, B. Delpech, *Int. J. Cancer* **1997**, *73*, 327.
[38] S. Bae, K. Ma, T. H. Kim, E. S. Lee, K. T. Oh, E. S. Park, K. C. Lee, Y. S. Youn, *Biomaterials* **2012**, *33*, 1536.
[39] H. H. Jiang, T. H. Kim, S. Lee, X. Chen, Y. S. Youn, K. C. Lee, *Biomaterials* **2011**, *32*, 8529.
[40] Z. P. Zhen, W. Tang, H. M. Chen, X. Lin, T. Todd, G. Wang, T. Cowger, X. Y. Chen, J. Xie, *ACS Nano* **2013**, *7*, 4830.
[41] G. Haran, R. Cohen, L. K. Bar, Y. Barenholz, *Biochim. Biophys. Acta* **1993**, *1151*, 201.
[42] I. A. Khalil, K. Kogure, S. Futaki, S. Hama, H. Akita, M. Ueno, H. Kishida, M. Kudoh, Y. Mishina, K. Kataoka, M. Yamada, H. Harashima, *Gene Ther.* **2007**, *14*, 682.
[43] Z. Gu, M. Yan, B. Hu, K. I. Joo, A. Biswas, Y. Huang, Y. Lu, P. Wang, Y. Tang, *Nano Lett.* **2009**, *9*, 4533.
[44] V. P. Torchilin, R. Rammohan, V. Weissig, T. S. Levchenko, *Proc. Natl. Acad. Sci. USA* **2001**, *98*, 8786.
[45] S. Futaki, T. Suzuki, W. Ohashi, T. Yagami, S. Tanaka, K. Ueda, Y. Sugiura, *J. Biol. Chem.* **2001**, *276*, 5836.
[46] C. E. Ashley, E. C. Carnes, G. K. Phillips, D. Padilla, P. N. Durfee, P. A. Brown, T. N. Hanna, J. Liu, B. Phillips, M. B. Carter, N. J. Carroll, X. Jiang, D. R. Dunphy, C. L. Willman, D. N. Petsev, D. G. Evans, A. N. Parikh, B. Chackerian, W. Wharton, D. S. Peabody, C. J. Brinker, *Nat. Mater.* **2011**, *10*, 389.
[47] G. J. Doherty, H. T. McMahon, *Annu. Rev. Biochem.* **2009**, *78*, 857.
[48] R. Mo, Q. Sun, J. Xue, N. Li, W. Li, C. Zhang, Q. Ping, *Adv. Mater.* **2012**, *24*, 3659.
[49] R. Mo, Q. Sun, N. Li, C. Zhang, *Biomaterials* **2013**, *34*, 2773.
[50] R. B. Campbell, D. Fukumura, E. B. Brown, L. M. Mazzola, Y. Izumi, R. K. Jain, V. P. Torchilin, L. L. Munn, *Cancer Res.* **2002**, *62*, 6831.